Comparison of primary aerosol emission and secondary aerosol formation from gasoline direct injection and port fuel injection vehicles

Zhuofei Du[1], Min Hu[1,3*], Jianfei Peng[1†], Wenbin Zhang[2], Jing Zheng[1], Fangting Gu[1], Yanhong Qin[1], Yudong Yang[1], Mengren Li[1], Yusheng Wu[1], Min Shao[1], Shijin Shuai[2]

1. State Key Joint Laboratory of Environmental Simulation and Pollution Control, College of Environmental Sciences and Engineering, Peking University, Beijing 100871, China

2. State Key Laboratory of Automotive Safety and Energy, Department of Automotive Engineering, Tsinghua University, Beijing 100084, China

3. Beijing Innovation Center for Engineering Sciences and Advanced Technology, Peking University, Beijing 100871, China

[†] Now at Department of Atmospheric Sciences, Texas A&M University, College Station, TX 77843, US

*Corresponding author: Min Hu, minhu@pku.edu.cn

Abstract

Gasoline vehicles ~~greatly~~ contribute to urban particulate matter (PM) pollution. Gasoline direct injection (GDI) engines, known as their higher fuel efficiency than that of port fuel injection (PFI) engines, have been increasingly employed in new gasoline vehicles. However, the impact of this trend on air quality is still poorly understood. Here, we investigated both primary emissions and secondary organic aerosol (SOA) formation from GDI and PFI vehicles under urban-like condition, using combined approaches involving chassis dynamometer measurement and environmental chamber simulation. The PFI vehicle emits slightly more volatile organic compounds, e.g., benzene and toluene, whereas the GDI vehicle emits more particulate components, e.g., the total PM, elemental carbon, primary organic aerosols and polycyclic aromatic hydrocarbons. Strikingly, a much higher SOA production (by a factor of approximately 2.7) ~~is found~~ from the exhaust of the GDI vehicle than that of the PFI vehicle under the

same conditions. More importantly, the higher SOA production found in the GDI vehicle exhaust occurs concurrently with lower concentrations of traditional SOA precursors, e.g., benzene and toluene, indicating a greater contribution of intermediate volatility organic compounds and semivolatile organic compounds in the GDI vehicle exhaust to the SOA formation. Our results highlight the considerable potential contribution of GDI vehicles to urban air pollution in the future.

1 Introduction

Organic aerosols account for approximately 20-50 % of ambient fine particulate matter ($PM_{2.5}$), with significant environment and health effects (Kanakidou et al., 2005). Primary organic aerosol (POA) is emitted directly by sources, while secondary organic aerosol (SOA) is mainly formed via oxidation of gaseous precursors in the atmosphere and account for about 30-90 % of the organic aerosol (OA) mass worldwide (Zhang et al., 2007; Hu et al., 2016), but SOA source remain poorly constrained. Robinson et al. (2007) proposed that low-volatility gas-phase species emitted from diesel vehicles were important sources for urban ambient SOA, which achieved better mass closure between observed and modeled SOA. Using an updated CMAQ model, Jathar et al. (2017) found that 30-40% OA was contributed from vehicles in the southern California, and half of which was SOA. Huang et al. (2014) recently revealed that 15-65 % of SOA was contributed by fossil fuel consumption (i.e., traffic and coal burning) in megacities in China. These indicated that vehicles have important contribution to ambient SOA in urban areas. An ambient organic aerosol measurement in the Los Angeles Basin demonstrated that SOA contributed from gasoline vehicles was significant in the urban air, much larger than that from diesel vehicles (Bahreini et al., 2012). Similar conclusion was reached by Hayes et al. (2013) based on mass spectrometer results. Meanwhile, several chamber simulation studies concluded that exhaust of gasoline vehicles could form substantial SOA (Jathar et al., 2014). Thus, gasoline vehicles exhaust is highly associated with ambient SOA formation.

Gasoline vehicles can be categorized into two types based on the fuel injection technologies in their engines, i.e., port fuel injection (PFI) vehicles and gasoline direct injection (GDI) vehicles. Unlike a PFI engine, in which

gasoline is injected into intake port, gasoline is sprayed into cylinder directly in a GDI engine. With the increased atomization and vaporization rate of fuel, and more accurate control of fuel volume and injection time, a GDI engine has many advantages, such as better fuel efficiency, lower CO_2 emissions and less fuel pumping loss (Alkidas, 2007; Myung et al., 2012; Liang et al., 2013). In past decades, PFI vehicles dominated the market share of gasoline cars in the world. However, in recent years, GDI vehicles have been increasingly employed, due to their higher fuel efficiency. The market share of GDI vehicles in sales in 2016 reached about 25 %, 50 % and 60 % in China, the US and Europe, respectively (Wen et al., 2016; Zimmerman et al., 2016).

Several previous studies investigated the emissions of GDI and PFI vehicles, in terms of concentrations of gaseous pollutants, particle numbers and mass concentrations, and evaluated the reduction of emissions with ~~the~~ upgrading emission standards (Ueberall et al., 2015; Zhu et al., 2016; Saliba et al., 2017). These studies show that GDI vehicles emit more primary particles than PFI vehicles (Zhu et al., 2016; Saliba et al., 2017), and even diesel vehicles equipped with diesel particulate filter (DPF) (Wang et al., 2016), ~~which is~~ likely due to insufficient time allowed for gasoline fuel to be mixed with air thoroughly, as well as gasoline droplets impinging onto pistons and surfaces of combustion chamber in GDI engine (Chen et al., 2017; Fu et al., 2017). However, in most studies, vehicles were tested under the driving cycles of the US or European standards, ~~indicating that~~ those results ~~are~~ not representative of China's traffic conditions.

SOA production from gasoline vehicle exhaust was previously simulated in smog chambers and potential aerosol mass (PAM) flow reactors. SOA formed from gaseous pollutants exceeds the related POA emissions and having much more contribution to air quality degradation. These studies mostly focused on the impacts of SOA formation by the model year (Gordon et al., 2014; Jathar et al., 2014; Liu et al., 2015), fuel formulations (Peng et al., 2017), driving cycles (including idling) (Nordin et al., 2013; Platt et al., 2013) and start-up modes of the gasoline vehicles (Nordin et al., 2013). Few studies, however, have investigated SOA formation from vehicles with different engine technologies (GDI and PFI) under the same working condition.

In this study, both primary emissions and secondary aerosol formation from GDI and PFI vehicles were investigated. To represent typical urban driving patterns in megacities such as Beijing, the vehicles were tested

76 using gasoline fuel meeting the China Phase V fuel standard, and were operated with the cold-start Beijing cycle

77 (BJC). The SOA formation from both the PFI and GDI vehicle exhausts were then simulated using a smog chamber.

78 Finally, the overall contributions of the GDI and PFI gasoline vehicles to ambient particulate matter (PM) were

79 evaluated. This study is part of a project that investigates the relationship between vehicle (engine) emissions and

80 ambient aerosols, including potential of SOA formation from a PFI engine (Du et al., 2017) and the effects of

81 gasoline aromatics on SOA formation (Peng et al., 2017).

82

83 2 Materials and methods

84 2.1 Vehicles

85 One PFI vehicle and one GDI vehicle were tested in this study to investigate their primary emissions and SOA

86 formations. ~~In this study, the selected PFI and GDI~~ vehicles were certified to the China Phase IV Emissions

87 Standard (equivalent to Euro IV) and the China Phase V Emissions Standard (equivalent to Euro V), respectively.

88 More information of the vehicles is shown in Table 1. The fuel used in the experiments was a typical Phase V

89 gasoline on the China market (sulfur content = 6 mg kg^{-1}). More information of the fuel is provided in Table S1 in

90 the Supplement. Cold-start BJC, characterized by a higher proportion of idling periods and lower acceleration

91 speeds than the New European Driving Cycle (NEDC), was performed to simulate the repeated braking and

92 acceleration on road in megacities such as Beijing. The BJC lasted approximately 17 minutes, with a maximum

93 speed of 50 km h^{-1} (Peng et al., 2017).

94

95 2.2 Experimental setup

96 The chamber experiments were carried out in the summer at the State Key Laboratory of Automotive Safety

97 and Energy of Tsinghua University in Beijing, including two experiments conducted with GDI vehicle and four

98 experiments conducted with PFI vehicle. The tested vehicles were placed on a chassis dynamometer system (Burke

99 E. Porter Machinery Company) with a controlled room temperature ~~and absolute humidity~~ of 26.4±2.5 °C ~~and~~

100 11.5±2.4 g m^{-3}, ~~respectively.~~ The exhaust emitted by the vehicle tailpipe was diluted in a constant volume sampler

101 (CVS) system, where the flow was maintained at 5.5 m^3 min^{-1} using filtered ambient air, achieving about 20 ~~times~~

102 dilution of the exhaust. Several instruments, including an AVL CEBII gas analyzer, a Cambustion Differential

103 Mobility Spectrometer (DMS500) and a particle sampler, were connected to the CVS (detailed in Figure 1 and

104 section 2.3) to characterize the primary gas- and particulate-phase pollutants. The diluted exhaust~~s~~ produced by the

105 CVS system ~~were~~ injected into an outdoor chamber, where secondary aerosol formation ~~from gasoline vehicle~~

106 ~~exhausts~~ was simulated. This was the second dilution step of the exhaust~~s~~ and had a dilution factor of approximately

107 15. A schematic illustration of the outdoor experimental setup is shown in Figure 1.

108   The photochemical oxidation experiments were carried out in a quasi-atmospheric aerosol evolution study

109 (QUALITY) outdoor chamber. More details of the setup and performance of the QUALITY chamber were

110 introduced by Peng et al. (2017). Prior to each experiment, the chamber was covered with a double-layer anti-

111 ultraviolet (anti-UV) shade to block sunlight and was cleaned with zero air for about 15 h to create a clean

112 environment. Approximately 120 ppb O_3 were injected into the chamber prior to the injection of vehicle exhaust to

113 make the oxidation environment similar to the mean O_3 peak concentration in the ambient atmosphere. Before the

114 chamber was exposed to sunlight, about 15-minute period was left to ensure that the pollutants mixed sufficiently

115 in the chamber, then the initial concentrations were characterized in the dark. Subsequently, the anti-UV shade

116 ~~were~~ removed from the chamber and photo-oxidation was initiated. A suite of high time resolution instruments was

117 utilized to track the evolution of pollutants during the chamber experiments. Zero air was added into the chamber

118 when sampling to maintain a constant pressure.

119

120 2.3 Instrumentation

121   Primary gases and aerosols were measured by the instruments connected to the CVS. The concentrations of

122 gaseous pollutants, including CO, CO_2, NO_x and total hydrocarbon (THC) were monitored with a gas analyzer

123 AVL Combustion Emissions Bench II (CEB II, AVL, Austria). Primary aerosols were measured with both on-line

124 and off-line instruments. A DMS500 (Cambustion, UK) was implemented to monitor the real-time number size

125 distribution and total number concentration of primary particles. Its sampling line was heated to maintain the

126 temperature at 150℃. The aerosols were also collected on Teflon and quartz filters by AVL Particulate Sampling

127 System (SPC472, AVL, Austria) to analyze the mass, organic carbon (OC) and elemental carbon (EC) emission

128 factors using a balance and OC/EC analyzer (Sunset Lab, USA).

129 During the chamber experiments, a suite of real-time instruments was utilized to characterize the evolutions

130 of the gas and particulate-phase pollutants. CO analyzer, NO-NO$_2$-NO$_x$ analyzer and O$_3$ analyzer (Thermo Fisher

131 Scientific Inc., USA) were employed to measure the concentrations of CO, NO$_x$ (including NO and NO$_2$) and O$_3$,

132 respectively. The evolutions of volatile organic compounds (VOCs) were monitored with a proton transfer reaction

133 mass spectrometer (PTR-MS, IoniconAnalytik, Austria) (Lindinger et al., 1998). H$_3$O$^+$ was used as the reagent ion,

134 which reacted with the target compounds. The resulting ions were detected by a quadruple mass spectrometer.

135 Meanwhile, the particles size distribution was characterized using a scanning mobility particle sizer system (SMPS,

136 TSI, USA), which consisted of a differential mobility analyzer (DMA, TSI, USA) and a condensation particle

137 counter (CPC, TSI, USA). This system can measure aerosols with a diameters ranging from 15 nm to 700 nm. A

138 high-resolution time-of-flight aerosol mass spectrometer (HR-Tof-AMS, Aerodyne Research, USA) was applied to

139 obtain mass concentrations and size distributions of submicron, non-refractory aerosols, including sulfate, nitrate,

140 ammonium, chloride and organic (DeCarlo et al., 2006). Table 2 lists the instruments used to measure the primary

141 emissions and their evolutions in the chamber experiments.

142

143 **3 Results**

144 **3.1 Primary emissions**

145 **Gaseous pollutant emissions**

146 Emission factors (EFs) of CO$_2$, THC, benzene and toluene from the GDI and PFI vehicles are listed in Table

147 3. The EFs of CO$_2$ and THC are derived from measured concentrations in CVS, while the EFs of benzene and

148 toluene were calculated from the initial concentrations in the chamber. The THC emission factor was reported in

149 units of carbon mass, g C kg$^-$fuel^{-1}.

150 The GDI vehicle emitted less CO$_2$ and THC than the PFI vehicle due to their different fuel injection strategies

151 and mixing features (Liang et al. 2013; Gao et al., 2015). The EF of THC from the GDI vehicle met the standard

152 of the China Phase V Emission Standard (0.1 g km^{-1}), but that from the PFI vehicle was slightly ~~beyond~~ the standard

153 limit. The PFI vehicle used in this study met ~~lower~~ emission standard (the China Phase IV), which might cause

154 additional THC emission when compared to the China Phase V Emission Standard. In addition, ~~BJC and NEDC~~

155 ~~were applied in this study and emission standard, respectively.~~ More repeated braking and acceleration in BJC

156 might cause incomplete combustion and consequently higher THC emission from the PFI vehicle in this study. As

157 typical VOC species emitted by vehicles, benzene and toluene were measured in this study. For both vehicles, the

158 EFs of toluene were higher than those of benzene. Consistent with the feature of THC emission, the PFI vehicle

159 emitted more benzene and toluene than the GDI vehicle, and the enhancement of toluene was much larger than that

160 of benzene.

161 The EFs of the gaseous pollutants in this study had similar magnitudes to those in previous studies in which

162 gasoline vehicles met comparable levels of emission standards and were tested under cold-start driving condition,

163 while the results in this study were slightly higher, as shown in Table 3. This difference might be because the

164 California ultralow-emission vehicles (ULEV) (Saliba et al., 2017) and most LEV II vehicles (manufactured in

165 2004 or later) (May et al., 2014) meet the US certification gasoline emission standards for the ULEV category,

166 which has a lower limit of gaseous pollutants than the China Phase V Emission Standard. In addition, the different

167 driving cycles of our study and those other studies (listed in Table 3) might be another explanation for the difference

168 in the EFs of gaseous pollutants.

169 **Primary particle emissions**

170 The EFs of PM, elemental carbon (EC), POA and particulate polycyclic aromatic hydrocarbons (PAHs) are

171 shown in Table 4. The EF of PM$_{2.5}$ from the GDI vehicle was about 1.4 times higher than that of the PFI vehicle.

172 Both vehicles met the China Phase V Emission Standard for PM emission (4.5 mg km^{-1}). The GDI vehicle emitted

173 about 3.3 times more EC and 1.2 times more POA than the PFI vehicle. The primary carbonaceous aerosols

174 (EC+POA) accounted for 85 % and 82 % of the PM in the GDI and PFI vehicles respectively, suggesting that

175 carbonaceous aerosols were the major contributors in the PM from gasoline vehicles, especially for the GDI vehicle.

PAHs account for a small fraction of particulate organic matter in the atmosphere, but the molecular signature of PAHs can be utilized in source identification of vehicle emissions (Kamal et al., 2015). The GDI vehicle emitted about 1.5 times the PAHs of the PFI vehicle. The EFs of PAH compounds are listed in Table S2 in the Supplement, and details of PAHs measurement was described in Li et al. (2016). It should be noted that the PAHs were tested under warm-start cycles. A higher EF of PAHs would be obtained under cold-start cycle, since the lower temperature led to inefficient catalyst at the beginning of cold-start (Mathis et al., 2005). The main contributors to total PAHs mass emitted from gasoline vehicle exhaust in this study, especially from the GDI vehicle exhaust, was similar with the results reported by previous studies (Schauer et al., 2002; Hays et al., 2013).

The lower $PM_{2.5}$ and POA emissions from GDI vehicle were found in previous studies, except that a little higher $PM_{2.5}$ emission from GDI vehicle was illustrated in Saliba's study (Platt et al., 2013; May et al., 2014; Zhu et al., 2016; Saliba et al., 2017). The EC emissions were in the range of those of previous studies but on the lower level. The EF of the POA measured in this study was higher than those of other studies, leading to a higher OC/EC ratio, which could be attributed to the less strict emission standard of our vehicles and the different driving cycles applied in the experiments.

The bimodal number size distributions of the primary PM from the vehicles measured by the DMS500 are shown in Figure 2. The particle distributions of the exhausts of the GDI and PFI vehicles illustrated similar patterns, with two peaks located at about 10 nm for nucleation mode and at 60-90 nm for accumulation mode, respectively, which are consistent with the results of previous studies (Maricq et al., 1999; Chen et al., 2017). The particle number size distribution of the exhausts of the GDI vehicle showed a similar pattern to that of the PFI vehicle, with a much higher number concentration that is consistent with the emission of more particle mass.

3.2 SOA formation from gasoline vehicle exhaust

The time-resolved concentrations of gases and particles during the chamber experiments are illustrated in Figure 3. Before removing the anti-UV shade, the initial concentrations of NO_x, benzene and toluene from the PFI and GDI vehicles were 80 ppb, 3 ppb, 5 ppb and 100 ppb, 4 ppb, 14 ppb respectively.

201 After the aging experiment started (t=0 in Figure 3), NO was formed from NO_2 photolysis, and then reacted

202 with O_3 to form NO_2. The O_3 concentration increased rapidly to a maximum within 2-3 h and then decreased via

203 reactions and dilution. Benzene and toluene decayed during the aging process at different rates.

204 New particle formation was found inside the chamber 15 minutes after the exhaust was exposed to sunlight,

205 providing substantial seeds for secondary aerosol formation. Significant growths of particles in both size and mass

206 were observed in the chamber, indicating that a large amount of secondary aerosol was formed during the

207 photochemical oxidation. The chemical compositions of the secondary aerosols were measured continuously by

208 HR-Tof-AMS. Organic was the dominant composition of the secondary aerosol, accounting for 88-95 % of the

209 total particle mass inside the chamber (Figure S1), which is consistent with our previous research (Peng et al.,

210 2017). The SOA mass exhibited different growth rate for the two types of vehicles. After a 4 h oxidation in the

211 chamber, the SOA formed from the exhaust of the GDI vehicle was approximately double that of the PFI vehicle.

212 The solar radiation conditions significantly influenced the SOA formation. Thus, OH exposure was used to

213 characterize the photochemical age as a normalization, instead of the experiment time. Two VOC species with

214 noticeable differences in their reaction rate constants with OH radicals could be utilized to calculate the OH

215 exposure ([OH] Δt) based on Equation 1 (for benzene and toluene, as used in this study) (Yuan et al., 2012).

216 $[OH] \Delta t = \frac{1}{k_T - k_B} \times \left(\ln \frac{[T]}{[B]} \Big|_{t=0} - \ln \frac{[T\}}{[B]} \right)$  (1)

217 where k_T and k_B are the OH rate constants of benzene (1.2×10^{-12} cm^3 molecule^{-1} s^{-1}) (Yuan et al., 2012) and toluene

218 (5.5×10^{-12} cm^3 molecule^{-1} s^{-1}) (Kramp and Paulson, 1998), respectively. $\frac{[T]}{[B]}\Big|_{t=0}$ is the concentration ratio of

219 toluene to benzene at the beginning of the aging process, and $\frac{[T]}{[B]}$ is their concentration ratio measured during

220 aging process.

221 The SOA concentrations as a function of OH exposure are illustrated in Figure 4. Wall-loss correction and

222 dilution correction, including both particles and gaseous pollutants, were taken into consideration in the calculation

223 of the SOA mass concentration in the chamber. Detailed descriptions of corrections are given in the Supplement.

224 Assuming the mean OH concentration was 1.6×10^6 molecular cm^{-3} in Beijing (Lu et al., 2013), the whole aging

225 procedure in the chamber experiments was equal to a 6-10 h atmospheric photochemical oxidation. The average

226 SOA concentrations were 9.25 ± 1.80 and 4.68 ± 1.32 µg m^{-3} for the GDI and PFI vehicles, respectively, when the

227 OH exposure was 5×10^6 molecular cm^{-3} h in the chamber. Considering the driving cycle mileage and fuel

228 consumption, the SOA productions were 54.77 ± 10.70 mg kg-fuel^{-1} or 3.06 ± 0.60 mg km^{-1} for the GDI vehicle and

229 20.57 ± 5.82 mg kg-fuel^{-1} or 1.55 ± 0.44 mg km^{-1} for the PFI vehicle. Compared with the PFI vehicle, the GDI vehicle

230 exhaust exhibited a higher potential of SOA formation, even though the PFI vehicle emitted more VOCs, which

231 are considered as dominant class of SOA precursors. This result indicates that higher concentrations of some other

232 SOA precursors exist in the exhaust of GDI vehicles, which will be further discussed in section 3.3.

233 The results from chamber simulation of SOA formation from individual gasoline vehicles are illustrated in

234 Figure 5. The SOA production from the both vehicles in this study is in the range of the results of previous studies

235 (Nordin et al., 2013; Platt et al., 2013; Jathar et al., 2014; Liu et al., 2015; Peng et al., 2017). The variation of the

236 SOA production among these studies might be caused by several factors: the model years of vehicles

237 (corresponding to emission standards) (Nordin et al., 2013; Liu et al., 2015), their driving cycles (Nordin et al.,

238 2013), the initial concentrations of gaseous pollutants in the chamber (Jathar et al., 2014), and the ratio of VOCs to

239 NO$_x$ (Zhao et al., 2017) in the chamber experiments.

240 To investigate the dominant contributors to ambient PM from the GDI and PFI vehicles, Figure 6 illustrates

241 the EFs of EC and POA as well as the production factors of SOA in this study. The SOA production from the GDI

242 vehicle was approximately 2.7 times higher than that from the PFI vehicle. At 5×10^6 molecular cm^{-3} h OH exposure,

243 the SOA/POA ratio was approximately 1. Figure 4 illustrates that the SOA production increased with

244 photochemical age rapidly (within 2×10^7 molecular cm^{-3} h). Thus, SOA would exceed POA at higher OH exposure,

245 e.g., the SOA/POA ratio reached about 4 at 10^7 molecular cm^{-3} h OH exposure, becoming the major PM contributor.

246 In terms of the POA and EC emissions as well as the SOA formation, the GDI vehicle contributed 2.2 times more

247 than the PFI vehicle.

248 Although particle wall-loss correction as well as particle and gas dilution corrections were considered in this

249 study, several factors may still contribute to the uncertainties of the SOA productions. First, the ~~deposition~~ of semi-

250 volatile vapors to the chamber walls was not corrected, which may result in an underestimation of the rate of SOA

251 production with a factor of 1.1-4.1 (Zhang et al., 2014). Second, under some ambient conditions such as severe

252 urban haze events (Guo et al., 2014), particle mass concentrations can be as high as 200-300 $\mu g \ m^{-3}$, much higher

253 than the 23 ± 6 $\mu g \ m^{-3}$ under the chamber condition in this study. High particle mass loadings are favorable for the

254 partition of semi-volatile compounds into the particle phase, potentially increasing the rate of SOA production

255 (Odum et al., 1996). Third, stronger partitioning of SOA precursors into the particle phase may reduce the oxidized

256 products in the gas phase, which will potentially reduce the rate of SOA production (Seinfeld et al., 2003)

257

258 **3.3 SOA mass closure**

259 SOA production ($\Delta OA_{predicted}$) estimated from VOC precursors can be defined as Eq. (2):

260 $$\Delta OA_{predicted} = \sum_i (\Delta_i \times Y_i) \qquad (2)$$

261 where Δ_i is the concentration change of precursor VOC_i measured with PTR-MS in the chamber experiments, and

262 Y_i is the SOA yield of the VOC_i. In this study, benzene, toluene, C8 benzene and C9 benzene were involved in the

263 estimation of SOA production, and alkanes and alkenes were not considered. A recent study found that ozonolysis

264 of alkenes from gasoline vehicle exhaust could form SOA through aldol condensation reactions (Yang et al., 2018).

265 However, much low declines of concentrations were observed than those of aromatics during chamber experiments,

266 so alkenes might not play significant role in SOA formation in this study.

267 The SOA yield is sensitive to VOCs/NO$_x$ ratio (Song et al., 2005). In this study, the VOCs/NO$_x$ ratio was in

268 the range of 0.5-1.0 ppbC/ppb, thus, the SOA formation from the vehicle exhaust was determined under high NO$_x$

269 conditions. The high NO$_x$ SOA yields of benzene and toluene were taken from Ng et al. (2007). The C8 and C9

270 benzene used the SOA yield of m-xylene from Platt et al. (2013).

271 The increased predicted SOA contribution from the VOC precursors as a function of OH exposure

272 accumulation is demonstrated in Figure 7. At the end of the experiments, the SOA estimated from these speciated

273 VOCs accounted for about 25 % and 53 % of the measured SOA formation from the GDI and PFI vehicle exhausts,

274 respectively. Similar to the results of previous studies (Platt et al., 2013; Nordin et al., 2013; Gordon et al., 2014),

single-ring aromatics played an important role in the SOA formation, especially for the PFI vehicle which shows higher predicted SOA fraction.

The unpredicted fraction of the measured SOA in the chamber experiments was in the range of 47-75 %. Contributions from intermediate volatility organic compounds (IVOCs) and semivolatile organic compounds (SVOCs), e.g., long branched and cyclic alkanes and gas-phase polycyclic aromatic hydrocarbons could be a possible explanation for this underestimation. The SOA formed by oxidation of IVOCs and SVOCs is found to dominate over that from single-ring aromatics (Robinson et al., 2007; Zhao et al., 2016). The unpredicted SOA ratio exhibited a maximum value at the beginning of the experiment, indicating that the IVOCs and SVOCs with low volatilities produced SOA much more efficiently than the single-ring aromatics with high volatilities, as the first generation products of photo-oxidation of these precursors form SOA (Robinson et al., 2007).

The larger fraction of the unpredicted SOA from the GDI vehicle exhaust might be associated with higher IVOCs and SVOCs emissions. Gas-phase PAH is one of the main component of speciated IVOCs (Zhao et al., 2016). The particulate-phase PAHs from the GDI vehicle were more abundant than those from the PFI vehicle by a factor of 1.5 (section 3.1). Based on gas-particle equilibrium, this indicates that more gas-phase PAHs, including some aromatic IVOCs, might be emitted by the GDI vehicles, contributing to the SOA enhancement.

4 Discussions and conclusions

GDI and PFI vehicles have different fuel injection technologies in their engines, which affects their emissions of gaseous and particulate pollutants. In GDI engine, the fuel is directly injected into cylinder, which benefits the fuel atomization and vaporization and provides better control of fuel volume and the combustion process (Liang et al. 2013; Gao et al., 2015). Thus, in this study, the tested GDI vehicle has higher fuel economy and lower THC emission than the PFI vehicle. However, the insufficient mixing time allowed for the fuel and air leads to incomplete combustion in the GDI engine (Fu et al., 2014). In addition, direct fuel injection leads to fuel impingement onto surfaces of combustion chamber, where liquid pools form, favoring soot-like particulate formation (Ueberall et al., 2015; Chen et al., 2017). Consequently, larger particle mass and number are emitted by

the GDI vehicle than from the PFI vehicle. The particles emitted by the GDI vehicle have higher EC mass fraction, leading to lower OC/EC ratio. The considerable particle number emitted by gasoline vehicles, especially in GDI vehicles exhaust, makes a significant contribution to particle number concentration as well as seeds for further reactions in the atmosphere, and needs to be controlled in the future emission standards.

Our results show that the GDI vehicle contributes more to both primary and secondary aerosol than the PFI vehicle, and has greater impact on environment and air quality. In recent years, the market share of GDI vehicles exerts a continuous growth in China because they provide better fuel economy and lower CO_2 emissions. In 2016, GDI vehicles accounted for 25 % of China's market share in sales, and this proportion is expected to reach 60 % by 2020 (Wen et al., 2016). The PM enhancement of GDI vehicles with increasing population could potentially offset any PM emission reduction benefits, including the development of gasoline emission and fuel standards and the advanced engine technologies of gasoline vehicles. Therefore, our results highlight the necessity of further research and regulation of GDI vehicles.

It should be pointed out that the SOA formation factors in this study are based on one GDI vehicle and one PFI vehicle. Some previous studies proposed that vehicles have variations even though they meet similar specification vehicles and use the same fuel (Gordon et al., 2014; Jathar et al., 2014). Thus more researches with more vehicles for each technology are needed on SOA formation from vehicle exhaust.

Primary emissions and secondary organic formation from one GDI vehicle and one PFI vehicle were investigated when driving under cold-start BJC. The primary PM emitted by the GDI vehicle was 1.4 times greater than that from the PFI vehicle and the SOA formation from the GDI vehicle exhaust was 2.7 times greater than that from the PFI vehicle exhaust for the same OH exposure. The SOA production factors were 54.77 ± 10.70 mg kg-fuel^{-1} or 3.06 ± 0.60 mg km^{-1} for the GDI vehicle and 20.57 ± 5.82 mg kg-fuel^{-1} or 1.55 ± 0.44 mg km^{-1} for the PFI vehicle at an OH exposure of 5×10^6 molecular cm^{-3} h, which is consistent with the values seen in previous studies. Considering the higher amounts of OA derived from primary emission and secondary formation, the GDI vehicle contribute considerably more to particle mass concentrations in the ambient air than the PFI vehicle.

The SOA formation was predicted from the gaseous precursors emitted by the GDI and PFI vehicles under

high NO_x condition. Single-ring aromatic VOCs could explain only 25-53 % of the measured SOA formation in the chamber experiments. The GDI vehicle exhibited higher fraction of unexplained SOA. More IVOCs and SVOCs were inferred as being emitted by the GDI vehicle.

With increasing population of GDI vehicles, any benefits of the aerosol emission reduction of gasoline vehicles are substantially offset, because GDI vehicles have significant contributions to ambient aerosols. More work is needed to improve the understanding of GDI vehicle emissions and to provide information for the regulation of gasoline vehicles.

Data availability. The data presented in this article are available from the authors upon request (minhu@pku.edu.cn).

Acknowledgments

This work was supported by the National Basic Research Program of China (973 Program) (2013CB228503, 2013CB228502), National Natural Science Foundation of China (91544214, 41421064, 51636003), the Strategic Priority Research Program of Chinese Academy of Sciences (XDB05010500), China Postdoctoral Science Foundation (2015M580929), and the National Science and Technology Support Program (2014BAC21B01). We also thank the State Key Lab of Automotive Safety and Energy at Tsinghua University for the support to experiments.

346 **Reference**

347 Alkidas, A. C.: Combustion advancements in gasoline engines, Energy Conversion and Management, 48, 2751-

348 2761, 10.1016/j.enconman.2007.07.027, 2007.

349 Bahreini, R., Middlebrook, A. M., de Gouw, J. A., Warneke, C., Trainer, M., Brock, C. A., Stark, H., Brown, S. S.,

350 Dube, W. P., Gilman, J. B., Hall, K., Holloway, J. S., Kuster, W. C., Perring, A. E., Prevot, A. S. H., Schwarz, J. P.,

351 Spackman, J. R., Szidat, S., Wagner, N. L., Weber, R. J., Zotter, P., and Parrish, D. D.: Gasoline emissions dominate

352 over diesel in formation of secondary organic aerosol mass, Geophysical Research Letters, 39,

353 10.1029/2011gl050718, 2012.

354 Chen, L., Liang, Z., Zhang, X., and Shuai, S.: Characterizing particulate matter emissions from GDI and PFI

355 vehicles under transient and cold start conditions, Fuel, 189, 131-140, 10.1016/j.fuel.2016.10.055, 2017.

356 DeCarlo, P. F., Kimmel, J. R., Trimborn, A., Northway, M. J., Jayne, J. T., Aiken, A. C., Gonin, M., Fuhrer, K.,

357 Horvath, T., Docherty, K. S., Worsnop, D. R., and Jimenez, J. L.: Field-deployable, high-resolution, time-of-flight

358 aerosol mass spectrometer, Analytical Chemistry, 78, 8281-8289, 10.1021/ac061249n, 2006.

359 Du, Z., Hu, M., Peng, J., Guo, S., Zheng, R., Zheng, J., Shang, D., Qin, Y., Niu, H., Li, M., Yang, Y., Lu, S., Wu,

360 Y., Shao, M., and Shuai, S.: Potential of secondary aerosol formation from Chinese gasoline engine exhaust, Journal

361 of environmental sciences, 2017, in press.

362 Fu, H., Wang, Y., Li, X., and Shuai, S.: Impacts of Cold-Start and Gasoline RON on Particulate Emission from

363 Vehicles Powered by GDI and PFI Engines, SAE Technical Paper, 2014-01-2836, 10.4271/2014-01-2836, 2014.

364 Gao, Z., Curran, S. J., Parks, J. E., II, Smith, D. E., Wagner, R. M., Daw, C. S., Edwards, K. D., and Thomas, J. F.:

365 Drive cycle simulation of high efficiency combustions on fuel economy and exhaust properties in light-duty

366 vehicles, Applied Energy, 157, 762-776, 10.1016/j.apenergy.2015.03.070, 2015.

367 Gentner, D. R., Jathar, S. H., Gordon, T. D., Bahreini, R., Day, D. A., El Haddad, I., Hayes, P. L., Pieber, S. M.,

368 Platt, S. M., de Gouw, J., Goldstein, A. H., Harley, R. A., Jimenez, J. L., Prevot, A. S. H., and Robinson, A. L.:

369 Review of Urban Secondary Organic Aerosol Formation from Gasoline and Diesel Motor Vehicle Emissions,

370 Environmental science & technology, 51, 1074-1093, 10.1021/acs.est.6b04509, 2017.

Gordon, T. D., Presto, A. A., May, A. A., Nguyen, N. T., Lipsky, E. M., Donahue, N. M., Gutierrez, A., Zhang, M., Maddox, C., Rieger, P., Chattopadhyay, S., Maldonado, H., Maricq, M. M., and Robinson, A. L.: Secondary organic aerosol formation exceeds primary particulate matter emissions for light-duty gasoline vehicles, Atmos. Chem. Phys. , 14, 4661-4678, 10.5194/acp-14-4661-2014, 2014.

Guo, S., Hu, M., Zamora, M. L., Peng, J., Shang, D., Zheng, J., Du, Z., Wu, Z., Shao, M., Zeng, L., Molina, M. J., and Zhang, R.: Elucidating severe urban haze formation in China, Proceedings of the National Academy of Sciences of the United States of America, 111, 17373-17378, 10.1073/pnas.1419604111, 2014.

Hayes, P. L., Ortega, A. M., Cubison, M. J., Froyd, K. D., Zhao, Y., Cliff, S. S., Hu, W. W., Toohey, D. W., Flynn, J. H., Lefer, B. L., Grossberg, N., Alvarez, S., Rappenglueck, B., Taylor, J. W., Allan, J. D., Holloway, J. S., Gilman, J. B., Kuster, W. C., De Gouw, J. A., Massoli, P., Zhang, X., Liu, J., Weber, R. J., Corrigan, A. L., Russell, L. M., Isaacman, G., Worton, D. R., Kreisberg, N. M., Goldstein, A. H., Thalman, R., Waxman, E. M., Volkamer, R., Lin, Y. H., Surratt, J. D., Kleindienst, T. E., Offenberg, J. H., Dusanter, S., Griffith, S., Stevens, P. S., Brioude, J., Angevine, W. M., and Jimenez, J. L.: Organic aerosol composition and sources in Pasadena, California, during the 2010 CalNex campaign, Journal of Geophysical Research-Atmospheres, 118, 9233-9257, 10.1002/jgrd.50530, 2013.

Hays, M. D., Preston, W., George, B. J., Schmid, J., Baldauf, R., Snow, R., Robinson, J. R., Long, T., and Faircloth, J.: Carbonaceous aerosols emitted from light-duty vehicles operating on gasoline and ethanol fuel blends, Environmental science & technology, 47, 14502-14509, 10.1021/es403096v, 2013.

Hu, W., Hu, M., Hu, W., Jimenez, J. L., Yuan, B., Chen, W., Wang, M., Wu, Y., Chen, C., Wang, Z., Peng, J., Zeng, L., and Shao, M.: Chemical composition, sources, and aging process of submicron aerosols in Beijing: Contrast between summer and winter, Journal of Geophysical Research-Atmospheres, 121, 1955-1977, 10.1002/2015jd024020, 2016.

Huang, R.-J., Zhang, Y., Bozzetti, C., Ho, K.-F., Cao, J.-J., Han, Y., Daellenbach, K. R., Slowik, J. G., Platt, S. M., Canonaco, F., Zotter, P., Wolf, R., Pieber, S. M., Bruns, E. A., Crippa, M., Ciarelli, G., Piazzalunga, A., Schwikowski, M., Abbaszade, G., Schnelle-Kreis, J., Zimmermann, R., An, Z., Szidat, S., Baltensperger, U.,

Haddad, I. E., and Prévôt, A. S. H.: High secondary aerosol contribution to particulate pollution during haze events in China, Nature, 10.1038/nature13774, 2014.

Ito, Y., Shimoda, T., Aoki, T., Yuuki, K., Sakamoto, H., Kato, K., Their, D., Kattouah, P., Ohara, E. and Vogt, C.: Next Generation of Ceramic Wall Flow Gasoline Particulate Filter with Integrated Three Way Catalyst, SAE Technical Paper 2015-01-1073, 2015, doi:10.4271/2015-01-1073, 2015.

Jathar, S. H., Gordon, T. D., Hennigan, C. J., Pye, H. O. T., Pouliot, G., Adams, P. J., Donahue, N. M., and Robinson, A. L.: Unspeciated organic emissions from combustion sources and their influence on the secondary organic aerosol budget in the United States, Proc. Natl. Acad. Sci. USA, 111, 10473-10478, 10.1073/pnas.1323740111, 2014.

Jathar, S. H., Woody, M., Pye, H. O. T., Baker, K. R., and Robinson, A. L.: Chemical transport model simulations of organic aerosol in southern California: model evaluation and gasoline and diesel source contributions, Atmospheric Chemistry and Physics, 17, 4305-4318, 10.5194/acp-17-4305-2017, 2017.

Kamal, A., Cincinelli, A., Martellini, T., and Malik, R. N.: A review of PAH exposure from the combustion of biomass fuel and their less surveyed effect on the blood parameters, Environmental Science and Pollution Research, 22, 4076-4098, 10.1007/s11356-014-3748-0, 2015.

Kanakidou, M., Seinfeld, J. H., Pandis, S. N., Barnes, I., Dentener, F. J., Facchini, M. C., Van Dingenen, R., Ervens, B., Nenes, A., Nielsen, C. J., Swietlicki, E., Putaud, J. P., Balkanski, Y., Fuzzi, S., Horth, J., Moortgat, G. K., Winterhalter, R., Myhre, C. E. L., Tsigaridis, K., Vignati, E., Stephanou, E. G., and Wilson, J.: Organic aerosol and global climate modelling: a review, Atmospheric Chemistry and Physics, 5, 1053-1123, 2005.

Kramp, F., and Paulson, S. E.: On the uncertainties in the rate coefficients for OH reactions with hydrocarbons, and the rate coefficients of the 1,3,5-trimethylbenzene and m-xylene reactions with OH radicals in the gas phase, Journal of Physical Chemistry A, 102, 2685-2690, 10.1021/jp973289o, 1998.

Li, M., Hu, M., Wu, Y., Qin, Y., Zheng, R., Peng, J., Guo, Q., Xiao, Y., Hu, W., Zheng, J., Du, Z., Xiao, J., Shuai, S.: Characteristics of Particulate Organic Matters Emissions from Gasoline Direct Injection Engine and Its Influence Factors, Proceedings of the Chinese Society of Electrical Engineering, 36, 4443-4451.

Liang, B., Ge, Y., Tan, J., Han, X., Gao, L., Hao, L., Ye, W., and Dai, P.: Comparison of PM emissions from a gasoline direct injected (GDI) vehicle and a port fuel injected (PFI) vehicle measured by electrical low pressure impactor (ELPI) with two fuels: Gasoline and M15 methanol gasoline, Journal of Aerosol Science, 57, 22-31, 10.1016/j.jaerosci.2012.11.008, 2013.

Lindinger, W., Hansel, A., and Jordan, A.: On-line monitoring of volatile organic compounds at pptv levels by means of proton-transfer-reaction mass spectrometry (PTR-MS) - Medical applications, food control and environmental research, International Journal of Mass Spectrometry, 173, 191-241, 10.1016/s0168-1176(97)00281-4, 1998.

Liu, T., Wang, X., Deng, W., Hu, Q., Ding, X., Zhang, Y., He, Q., Zhang, Z., Lü, S., Bi, X., Chen, J., and Yu, J.: Secondary organic aerosol formation from photochemical aging of light-duty gasoline vehicle exhausts in a smog chamber, Atmos. Chem. Phys. , 15, 9049-9062, 10.5194/acp-15-9049-2015, 2015.

Lu, K. D., Hofzumahaus, A., Holland, F., Bohn, B., Brauers, T., Fuchs, H., Hu, M., Häseler, R., Kita, K., Kondo, Y., Li, X., Lou, S. R., Oebel, A., Shao, M., Zeng, L. M., Wahner, A., Zhu, T., Zhang, Y. H., and Rohrer, F.: Missing OH source in a suburban environment near Beijing: observed and modelled OH and HO_2 concentrations in summer 2006, Atmos. Chem. Phys. , 13, 1057-1080, 10.5194/acp-13-1057-2013, 2013.

Maricq, M. M., Podsiadlik, D. H., and Chase, R. E.: Gasoline vehicle particle size distributions: Comparison of steady state, FTP, and US06 measurements, Environmental science & technology, 33, 2007-2015, 10.1021/es981005n, 1999.

Mathis, U., Mohr, M., and Forss, A. M.: Comprehensive particle characterization of modern gasoline and diesel passenger cars at low ambient temperatures, Atmospheric Environment, 39, 107-117, 10.1016/j.atmosenv.2004.09.029, 2005.

May, A. A., Nguyen, N. T., Presto, A. A., Gordon, T. D., Lipsky, E. M., Karve, M., Gutierrez, A., Robertson, W. H., Zhang, M., Brandow, C., Chang, O., Chen, S., Cicero-Fernandez, P., Dinkins, L., Fuentes, M., Huang, S.-M., Ling, R., Long, J., Maddox, C., Massetti, J., McCauley, E., Miguel, A., Na, K., Ong, R., Pang, Y., Rieger, P., Sax, T., Tin, T., Thu, V., Chattopadhyay, S., Maldonado, H., Maricq, M. M., and Robinson, A. L.: Gas- and particle-phase

primary emissions from in-use, on-road gasoline and diesel vehicles, Atmospheric Environment, 88, 247-260, 10.1016/j.atmosenv.2014.01.046, 2014.

Myung, C.-L., Kim, J., Choi, K., Hwang, I. G., and Park, S.: Comparative study of engine control strategies for particulate emissions from direct injection light-duty vehicle fueled with gasoline and liquid phase liquefied petroleum gas (LPG), Fuel, 94, 348-355, 10.1016/j.fuel.2011.10.041, 2012.

Ng, N. L., Kroll, J. H., Chan, A. W. H., Chhabra, P. S., Flagan, R. C., and Seinfeld, J. H.: Secondary organic aerosol formation from m-xylene, toluene, and benzene, Atmos. Chem. Phys. , 7, 3909–3922, 2007.

Nordin, E. Z., Eriksson, A. C., Roldin, P., Nilsson, P. T., Carlsson, J. E., Kajos, M. K., Hellén, H., Wittbom, C., Rissler, J., Löndahl, J., Swietlicki, E., Svenningsson, B., Bohgard, M., Kulmala, M., Hallquist, M., and Pagels, J. H.: Secondary organic aerosol formation from idling gasoline passenger vehicle emissions investigated in a smog chamber, Atmos. Chem. Phys. , 13, 6101-6116, 10.5194/acp-13-6101-2013, 2013.

Odum, J. R., Hoffmann, T., Bowman, F., Collins, D., Flagan, R. C., and Seinfeld, J. H.: Gas/particle partitioning and secondary organic aerosol yields, Environ. Sci. Technol., 30, 2580-2585, 10.1021/es950943+, 1996.

Peng, J., Hu, M., Du, Z., Wang, Y., Zheng, J., Zhang, W., Yang, Y., Qin, Y., Zheng, R., Xiao, Y., Wu, Y., Lu, S., Wu, Z., Guo, S., Mao, H., and Shuai, S.: Gasoline aromatic: a critical determinant of urban secondary organic aerosol formation, Atmospheric Chemistry and Physics, 2017, in press.

Platt, S. M., El Haddad, I., Zardini, A. A., Clairotte, M., Astorga, C., Wolf, R., Slowik, J. G., Temime-Roussel, B., Marchand, N., Ježek, I., Drinovec, L., Močnik, G., Möhler, O., Richter, R., Barmet, P., Bianchi, F., Baltensperger, U., and Prévôt, A. S. H.: Secondary organic aerosol formation from gasoline vehicle emissions in a new mobile environmental reaction chamber, Atmos. Chem. Phys. , 13, 9141-9158, 10.5194/acp-13-9141-2013, 2013.

Robinson, A. L., Donahue, N. M., Shrivastava, M. K., Weitkamp, E. A., Sage, A. M., Grieshop, A. P., Lane, T. E., Pierce, J. R., and Pandis, S. N.: Rethinking organic aerosols: Semivolatile emissions and photochemical aging, Science, 315, 1259-1262, 10.1126/science.1133061, 2007.

Saliba, G., Saleh, R., Zhao, Y., Presto, A. A., Lambe, A. T., Frodin, B., Sardar, S., Maldonado, H., Maddox, C., May, A. A., Drozd, G. T., Goldstein, A. H., Russell, L. M., Hagen, F., and Robinson, A. L.: Comparison of Gasoline

Direct-Injection (GDI) and Port Fuel Injection (PFI) Vehicle Emissions: Emission Certification Standards, Cold-Start, Secondary Organic Aerosol Formation Potential, and Potential Climate Impacts, Environmental science & technology, 51, 6542-6552, 10.1021/acs.est.6b06509, 2017.

Schauer, J. J., Kleeman, M. J., Cass, G. R. and Simoneit, B. R. T.: Measurement of Emissions from Air Pollution Sources. 5. C1-C32 Organic Compounds from Gasoline-Powered Motor Vehicles, Environmental science & technology, 36, 1169-1180, 2002.

Seinfeld, J. H., Kleindienst, T. E., Edney, E. O., and Cohen, J. B.: Aerosol growth in a steady-state, continuous flow chamber: Application to studies of secondary aerosol formation, Aerosol Science and Technology, 37, 728-734, 10.1080/02786820390214954, 2003.

Song, C., Na, K. S., and Cocker, D. R.: Impact of the hydrocarbon to NOx ratio on secondary organic aerosol formation, Environ. Sci. Technol., 39, 3143-3149, 10.1021/es0493244, 2005.

Ueberall, A., Otte, R., Eilts, P., and Krahl, J.: A literature research about particle emissions from engines with direct gasoline injection and the potential to reduce these emissions, Fuel, 147, 203-207, 10.1016/j.fuel.2015.01.012, 2015.

Wang, Y., Zheng, R., Qin, Y., Peng, J., Li, M., Lei, J., Wu, Y., Hu, M., and Shuai, S.: The impact of fuel compositions on the particulate emissions of direct injection gasoline engine, Fuel, 166, 543-552, 10.1016/j.fuel.2015.11.019, 2016.

Wang, Z. B., Hu, M., Wu, Z. J., Yue, D. L., He, L. Y., Huang, X. F., Liu, X. G., and Wiedensohler, A.: Long-term measurements of particle number size distributions and the relationships with air mass history and source apportionment in the summer of Beijing, Atmospheric Chemistry and Physics, 13, 10159-10170, 10.5194/acp-13-10159-2013, 2013.

Wen, Y., Wang, Y., Fu, C., Deng, W., Zhan, Z., Tang, Y., Li, X., Ding, H., and Shuai, S.: The Impact of Injector Deposits on Spray and Particulate Emission of Advanced Gasoline Direct Injection Vehicle, SAE Technical Paper, 2016-01-2284, 10.4271/2016-01-2284, 2016.

494 Yang, B., Ma, P. K., Shu, J. N., Zhang, P., Huang, J. Y. and Zhang, H. X.: Formation mechanism of secondary

495 organic aerosol from ozonolysis of gasoline vehicle exhaust, Environmental Pollution, 234, 960-968,

496 10.1016/j.envpol.2017.12.048, 2018.

497 Yuan, B., Shao, M., de Gouw, J., Parrish, D. D., Lu, S., Wang, M., Zeng, L., Zhang, Q., Song, Y., Zhang, J., and

498 Hu, M.: Volatile organic compounds (VOCs) in urban air: How chemistry affects the interpretation of positive

499 matrix factorization (PMF) analysis, Journal of Geophysical Research: Atmospheres, 117, n/a-n/a,

500 10.1029/2012jd018236, 2012.

501 Zhang, Q., Jimenez, J. L., Canagaratna, M. R., Allan, J. D., Coe, H., Ulbrich, I., Alfarra, M. R., Takami, A.,

502 Middlebrook, A. M., Sun, Y. L., Dzepina, K., Dunlea, E., Docherty, K., DeCarlo, P. F., Salcedo, D., Onasch, T.,

503 Jayne, J. T., Miyoshi, T., Shimono, A., Hatakeyama, S., Takegawa, N., Kondo, Y., Schneider, J., Drewnick, F.,

504 Borrmann, S., Weimer, S., Demerjian, K., Williams, P., Bower, K., Bahreini, R., Cottrell, L., Griffin, R. J.,

505 Rautiainen, J., Sun, J. Y., Zhang, Y. M., and Worsnop, D. R.: Ubiquity and dominance of oxygenated species in

506 organic aerosols in anthropogenically-influenced Northern Hemisphere midlatitudes, Geophysical Research Letters,

507 34, 10.1029/2007gl029979, 2007.

508 Zhang, X., Cappa, C. D., Jathar, S. H., McVay, R. C., Ensberg, J. J., Kleeman, M. J., and Seinfeld, J. H.: Influence

509 of vapor wall loss in laboratory chambers on yields of secondary organic aerosol, Proc. Natl. Acad. Sci. USA, 111,

510 5802-5807, 10.1073/pnas.1404727111, 2014.

511 Zhao, Y., Nguyen, N. T., Presto, A. A., Hennigan, C. J., May, A. A., and Robinson, A. L.: Intermediate Volatility

512 Organic Compound Emissions from On-Road Gasoline Vehicles and Small Off-Road Gasoline Engines,

513 Environmental science & technology, 50, 4554-4563, 10.1021/acs.est.5b06247, 2016.

514 Zhao, Y., Saleh, R., Saliba, G., Presto, A. A., Gordon, T. D., Drozd, G. T., Goldstein, A. H., Donahue, N. M., and

515 Robinson, A. L.: Reducing secondary organic aerosol formation from gasoline vehicle exhaust, Proceedings of the

516 National Academy of Sciences of the United States of America, 114, 6984-6989, 10.1073/pnas.1620911114, 2017.

517 Zhu, R., Hu, J., Bao, X., He, L., Lai, Y., Zu, L., Li, Y., and Su, S.: Tailpipe emissions from gasoline direct injection

518 (GDI) and port fuel injection (PFI) vehicles at both low and high ambient temperatures, Environmental Pollution,

519 216, 223-234, 10.1016/j.envpol.2016.05.066, 2016.

520 Zimmerman, N., Wang, J. M., Jeong, C.-H., Ramos, M., Hilker, N., Healy, R. M., Sabaliauskas, K., Wallace, J. S.,

521 and Evans, G. J.: Field Measurements of Gasoline Direct Injection Emission Factors: Spatial and Seasonal

522 Variability, Environmental science & technology, 50, 2035-2043, 10.1021/acs.est.5b04444, 2016.

523

524 Table 1 Descriptions of the gasoline direct injection (GDI) and port fuel injection (PFI) vehicles used in the

525 experiments.

Vehicle	Make and model	Emission standard class	Model year	Mileage (km)	Displacement (cm^3)	Power (kW)	Weight (kg)
GDI	VW Sagitar	China V	2015	3000	1395	110	1395
PFI	Honda Civic	China IV	2009	42500	1799	103	1280

526

527 Table 2 Overview of all instruments used to measure the gas and particulate phase pollutants in the experiments.

Parameter	Phase	Instrument	Note
CO, CO_2, NO_x and total hydrocarbon (THC) concentration	Gas	Gas analyzer AVL Combustion Emissions Bench II	On-line
Aerosol number size distribution	Particle	DMS500	On-line
$PM_{2.5}$	Particle	Balance (AX105DR)	Off-line
Organic carbon/Elemental carbon concentration	Particle	OC/EC analyzer	Off-line
CO concentration	Gas	48i CO analyzer	On-line
NO, NO_2, and NO_x concentration	Gas	42i NO-NO_2-NO_x analyzer	On-line
O_3 concentration	Gas	49i O_3 analyzer	On-line
VOCs concentration	Gas	Proton transfer reaction mass spectrometer (PTR-MS)	On-line
Aerosol number (mass) size distribution	Particle	Scanning mobility particle sizer (SMPS, consist of 3081-DMA and 3775-CPC),	On-line
Size resolved non-refractory aerosol	Particle	High resolution time-of-flight aerosol mass spectrometer (HR-Tof-AMS)	On-line

528

529

530   Table 3 Emission factors (EFs) of gaseous pollutants from the gasoline direct injection (GDI) and port fuel injection (PFI) vehicles in

531   this study and those of previous studies.

	This study				Saliba et al., 2017		May et al., 2014	Platt et al., 2013		Zhu et al., 2016	
	GDI		PFI		GDI	PFI	PFI[a]			GDI	PFI
	China V		China IV		ULEV	ULEV	LEV II	Euro V		China IV	China IV
	Cold BJC				Cold UC[b]		Cold UC	Cold NEDC		Cold WLTC[c]	
	g kg-fuel^{-1}	g km^{-1}	g kg-fuel^{-1}	g km^{-1}	g km^{-1}	g km^{-1}	g kg-fuel^{-1}	g kg-fuel^{-1}	g km^{-1}	g km^{-1}	g km^{-1}
CO_2	3439 ±23	213 ±4	3350 ±24	283 ±4	-	-	-	-	-	187	215
THC	1.55 ±0.22	0.09 ±0.01	1.70 ±0.19	0.13 ±0.01	0.02	0.06	0.64	0.91-1.06	0.036-0.042	0.05	0.03
Benzene	0.056 ±0.011	0.003 ±0.001	0.061 ±0.016	0.005 ±0.001	-	-	0.018	-	0.002	-	-
Toluene	0.101 ±0.004	0.006 ±0.001	0.220 ±0.047	0.017 ±0.004	-	-	0.026	-	0.002	-	-

532   [a] 22 PFI vehicles and 3 GDI vehicles;

533   [b] UC: Unified Cycle;

534   [c] WLTC: Worldwide-harmonized Light-duty Test Cycle

535 Table 4 EFs of primary aerosols, including carbonaceous aerosols and particulate polycyclic aromatic hydrocarbons (PAHs) from the

536 GDI and PFI vehicles in this study and those of previous studies.

	This study				Saliba et al., 2017		May et al., 2014	Platt et al., 2013		Zhu et al., 2016	
	GDI		PFI		GDI	PFI	PFI			GDI	PFI
	China V		China IV		ULEV	ULEV	LEV II	Euro V		China IV	China IV
	Cold BJC				Cold UC		Cold UC	Cold NEDC		Cold WLTC	
	mg kg-fuel⁻¹	mg km⁻¹	mg kg-fuel⁻¹	mg km⁻¹	mg km⁻¹	mg km⁻¹	mg kg-fuel⁻¹	mg kg-fuel⁻¹	mg km⁻¹	mg km⁻¹	mg km⁻¹
PM$_{2.5}$	61.7±24.5	3.4±1.4	33.4±25.6	2.5±1.9	3.9	2.4	18.0	-	-	1.5	1.0
EC	10.7±3.6	0.6±0.2	2.4±1.6	0.2±0.1	3.0	0.6	12.2	11.2-20.0	1.2-1.7	-	-
POA	41.7±9.8	2.3±0.6	25.0±0.3	1.9±0.1	0.4	0.6	5.2	24.5-19.7	0.4-1.4	-	-
OC/EC	3.2		8.7		0.1	0.8	0.4	0.2-1.8		-	-
PAHs($\times10^6$)	20.4±2.1	1.1±0.1	13.2±4.1	1.0±0.3	-	-	-	-	-	-	-

537

538
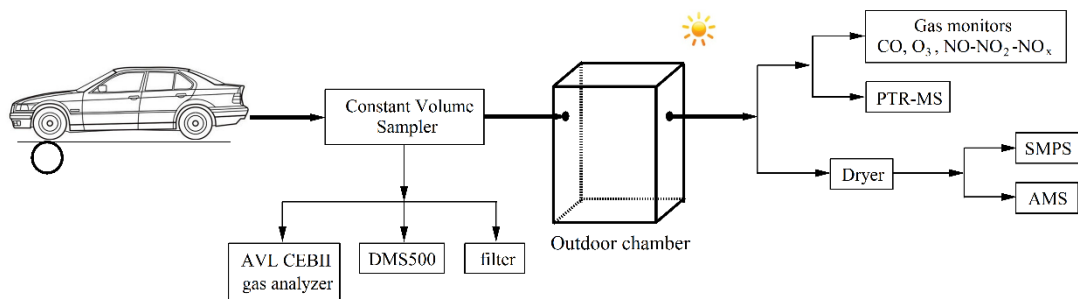
539

540   Figure 1. Schematic diagram of the outdoor chamber set up for the experiments.

541
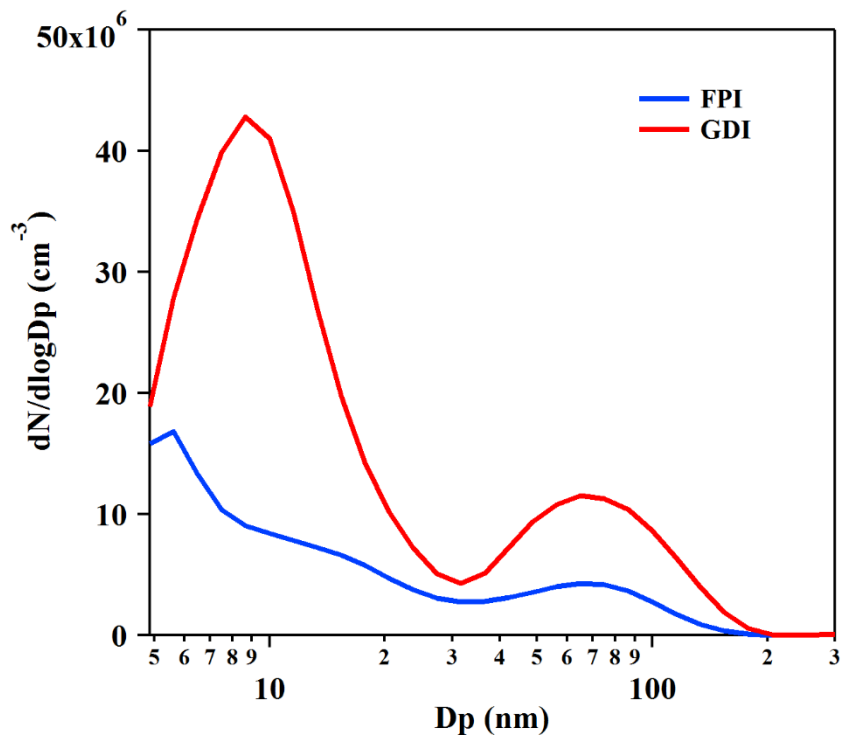
542

543 Figure 2. Number size distributions of primary PM emitted from the GDI (red line) and PFI (blue line) gasoline

544 vehicles. The results are average of particle number emissions from vehicles during a whole BJC, measured by

545 DMS500 in the CVS system. The particles were heated to 150℃ in the DMS500.

546
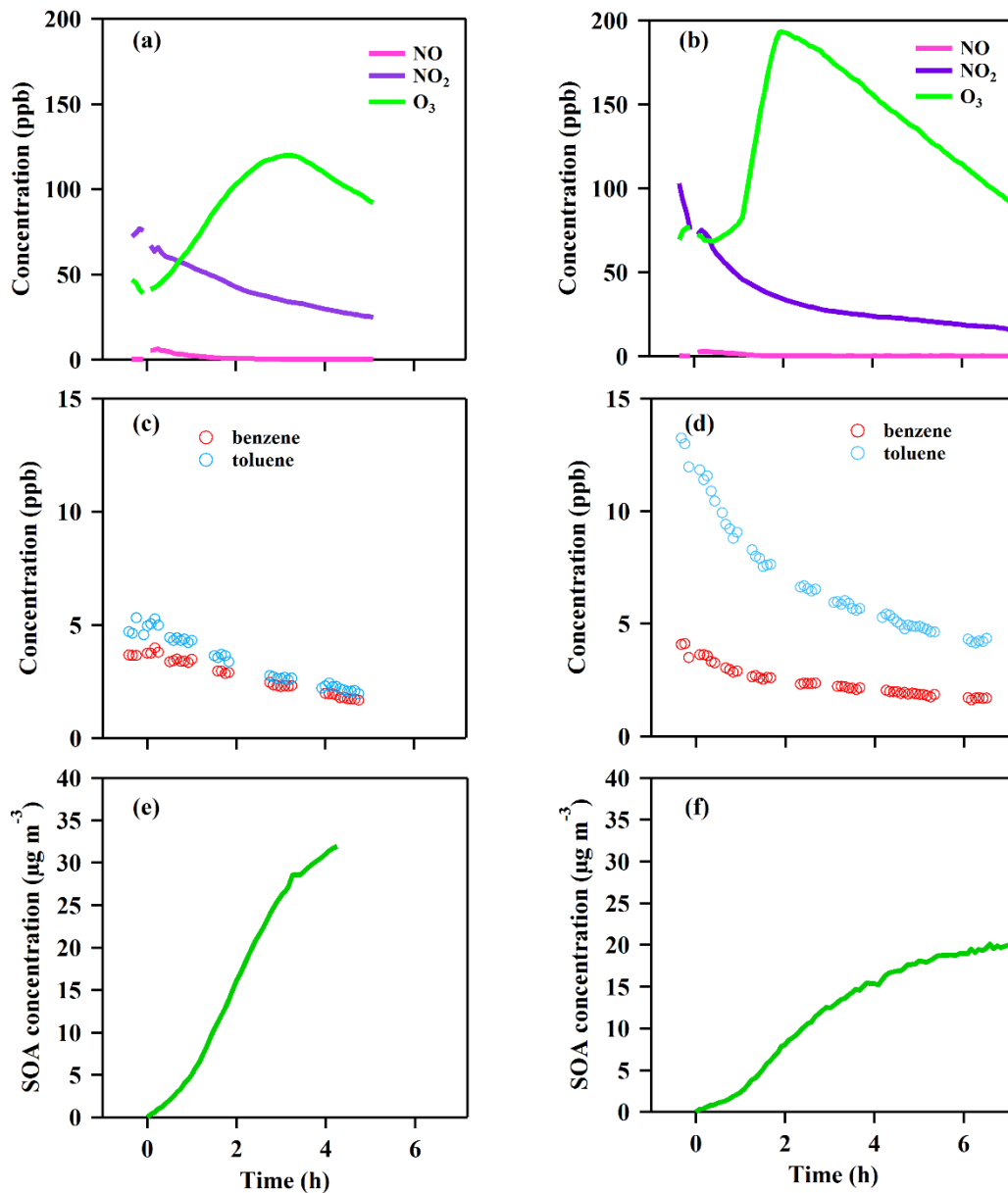
547

548 Figure 3. Time series of the gases and particle evolutions over the photochemical age in the chamber experiments

549 from the GDI vehicle exhaust (a, c, e) and PFI vehicle exhaust (b, d, f). (a, b): NO, NO_2 and O_3 concentration; (c,

550 d): benzene and toluene concentration; (e, f): corrected SOA concentration.

551

552
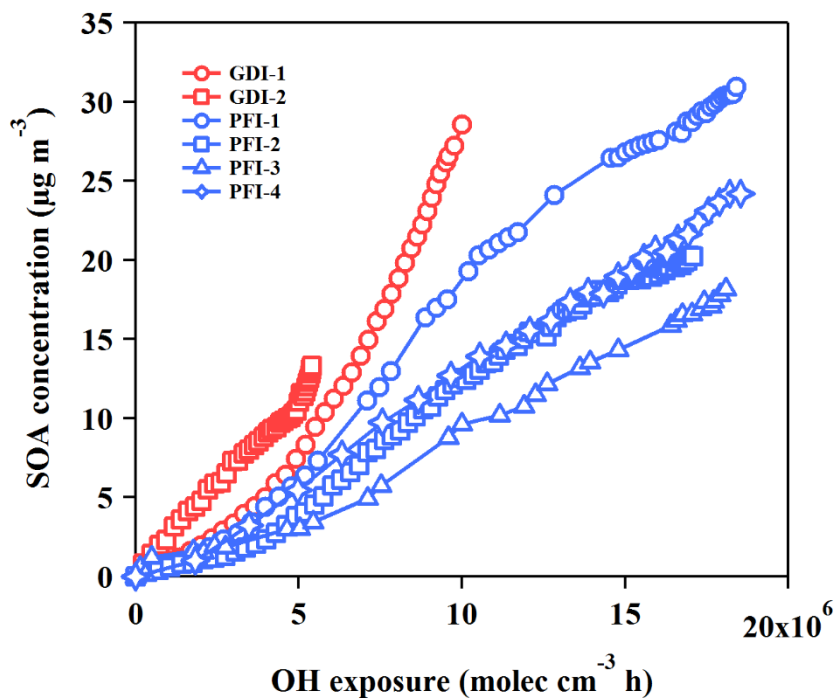
Figure 4. SOA productions from the GDI vehicle exhaust (red markers) and the PFI vehicle exhaust (blue markers)

as functions of OH exposure in the chamber experiments.

555

556
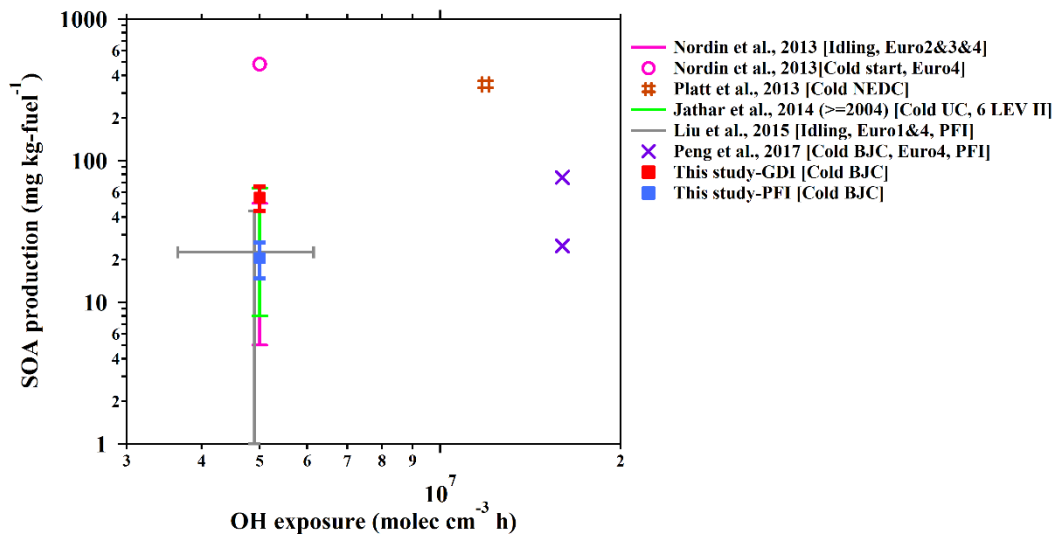
Figure 5. Fuel-based SOA production from gasoline vehicle exhaust as a function of OH exposure in the chamber

simulations. The SOA production data are from published studies of chamber simulation of gasoline vehicle

exhaust. From the study of Jathar et al. (2014), the SOA production of vehicles manufactured in 2004 or later (LEV

II) is selected, which is a model year that is more close to those of the vehicles in this study. The error bars of

previous results indicate the range of OH exposure (x axis) and SOA production (y axis) in their simulations. The

driving cycles and vehicle information are also noted in the legend of each study.

564
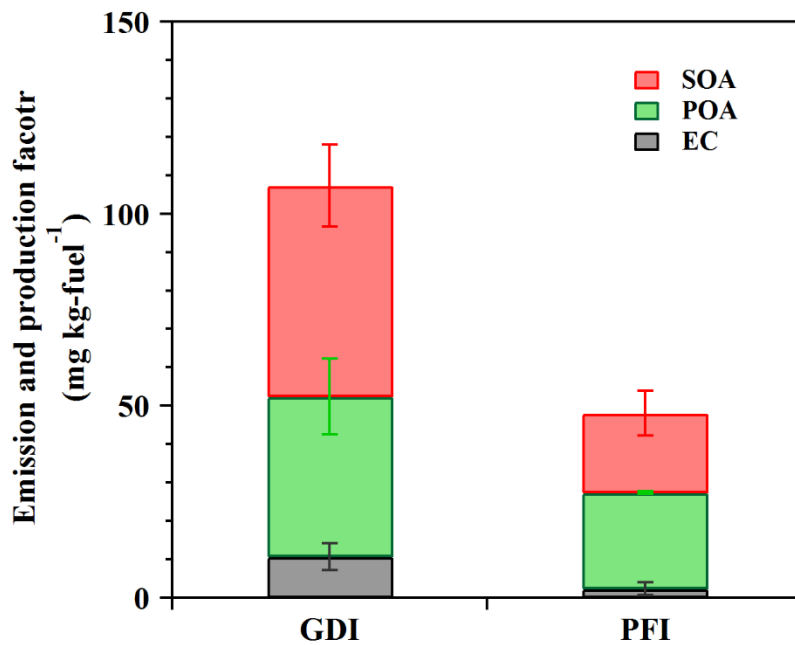
Figure 6 EC and POA EFs as well as corrected SOA production factors from the GDI and PFI vehicle exhausts in

this study (OH exposure = 5×10^6 molecular cm^{-3} h).

567
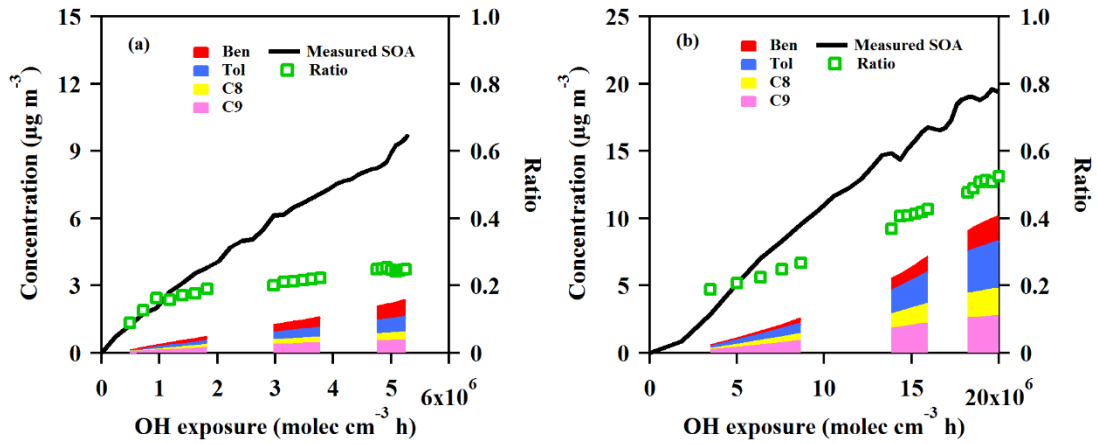
568

569 Figure 7. Measured and predicted SOA concentration as a function of OH exposure from GDI vehicle exhaust (a)

570 and PFI vehicle exhaust (b) in the chamber experiments. The black line is the measured SOA concentration with

571 wall-loss and particle dilution correction during the experiment. The red, blue, yellow and pink areas are predicted

572 SOA concentration estimated from benzene, toluene, C8 benzene and C9 benzene, respectively. The green markers

573 are the ratios of the predicted SOA to the measured SOA.

574